

Special Section: Nonuniform Flow across Vadose Zone Scales

Core Ideas

- Mass redistribution at unsaturated fracture intersections depends on free-surface flow modes.
- A Washburn-type flow regime is recovered via an analytical solution for capillary fracture inflow.
- A Gaussian transfer function predicts mass partitioning for arbitrary-sized fracture cascades.

Analogue Fracture Experiments and Analytical Modeling of Unsaturated Percolation Dynamics in Fracture Cascades

Torsten Noffz,* Marco Dentz, and Jannes Kordilla

Infiltration and recharge dynamics in fractured aquifer systems often strongly deviate from diffuse Darcy–Buckingham type flows due to the existence of a complex gravity-driven flow component along fractures, fracture networks, and fault zones. The formation of preferential flow paths in the unsaturated or vadose zone can trigger rapid mass fluxes, which are difficult to recover by volume-effective modeling approaches (e.g., the Richards equation) due to the nonlinear nature of free-surface flows and mass partitioning processes at unsaturated fracture intersections. In this study, well-controlled laboratory experiments enabled the isolation of single aspects of the mass redistribution process that ultimately affect travel time distributions across scales. We used custom-made acrylic cubes (20 by 20 by 20 cm) in analog percolation experiments to create simple wide-aperture fracture networks intersected by one or multiple horizontal fractures. A high-precision multichannel dispenser produced gravity-driven free-surface flow (droplets or rivulets) at flow rates ranging from 1 to 5 mL min⁻¹. Total inflow rates were kept constant while the fluid was injected via 15 (droplet flow) or three inlets (rivulet flow) to reduce the impact of erratic flow dynamics. Normalized fracture inflow rates were calculated and compared for aperture widths of 1 and 2.5 mm. A higher efficiency in filling an unsaturated fracture by rivulet flow observed in former studies was confirmed. The onset of a capillary-driven Washburn-type flow was determined and recovered by an analytical solution. To upscale the dynamics and enable the prediction of mass partitioning for arbitrary-sized fracture cascades, a Gaussian transfer function was derived that reproduces the repetitive filling of fractures, where rivulet flow is the prevailing regime. Results show good agreement with experimental data for all tested aperture widths.

Abbreviations: PMMA, poly(methyl methacrylate).

T. Noffz and J. Kordilla, Dep. of Applied Geology, Univ. of Göttingen, 37077 Göttingen, Germany; M. Dentz, Institute of Environmental Assessment and Water Research (IDAEA), Spanish National Research Council (CSIC), 08034 Barcelona, Spain. *Corresponding author (tnoffz@gwdg.de).

Received 17 Aug. 2018.

Accepted 31 Oct. 2018.

Citation: Noffz, T., M. Dentz, and J. Kordilla. 2019. Analogue fracture experiments and analytical modeling of unsaturated percolation dynamics in fracture cascades. *Vadose Zone J.* 18:180155. doi:10.2136/vzj2018.08.0155

© Soil Science Society of America. This is an open access article distributed under the CC BY-NC-ND license (<http://creativecommons.org/licenses/by-nc-nd/4.0/>).

Fractured porous media contribute to approximately 75% of global aquifers (Dietrich et al., 2005), highlighting their importance in the context of groundwater resources management. Furthermore, fractured rock formations have been the target of risk assessment measures that investigate their suitability as long-term waste repositories (e.g., for nuclear waste disposal; Evans and Rasmussen, 1991; Tsang et al., 2015). Given their heterogeneous nature on small and large scales, fractured rocks offer a domain for gravity-driven flow along preferential flow paths or zones even if the surrounding matrix is not fully saturated (Faybishenko et al., 2015; Nimmo, 2012). Channeled flows may occur near the surface in macropores of soils (Nimmo, 2012) or within widened fracture networks (Dahan et al., 1999, 2000; Kordilla et al., 2017) via dissolution shafts in strongly weathered karst systems (Gunn, 1981; Williams, 2008). Furthermore, they locally develop in talus and waste rock deposits (Tokunaga et al., 2005; Trinchero et al., 2011) and along fault zones (Bodvarsson et al., 1997; Liu et al., 2004), where they can strongly contribute to the overall flux of a system. However, classical volume-effective modeling approaches (e.g., the Richards equation) and associated relationships between system geometry and flow properties might not be suitable to recover the nonlinear flow and mass partitioning processes that control preferential flow dynamics and are still under investigation (e.g., Dippenaar and Van Rooy, 2016). Different flow regimes, e.g., droplet, rivulet, and film

flow, can coexist even in controlled settings and are difficult to cast into unified conceptual frameworks (Ghezzehei, 2004).

In well-controlled analog percolation experiments, the fracture-specific formation of flow modes and instabilities (Jones et al., 2018; Li et al., 2018) and the role of unsaturated fracture intersections on partitioning behavior has been investigated (e.g., Ji et al., 2006; Kordilla et al., 2017; LaViolette et al., 2003; Nicholl and Glass, 2005; Wood et al., 2002, 2005; Wood and Huang, 2015), where the applied flow rate controls the stability of a desired flow regime (Towell and Rothfeld, 1966; Schmuki and Laso, 1990). These studies emphasize the importance of fracture intersections as capillary barriers (until steady-state conditions are established), which may induce pulsating flows and act as important integrators for dispersion and recharge processes. In an earlier study (Kordilla et al., 2017), we showed how flow modes affect the mass partitioning process at an unsaturated fracture intersection. The numerical simulations and laboratory experiments have demonstrated that a considerably larger bypass efficiency is observed for droplet flows (Fig. 1). Additionally, a transition of fracture inflow from plug flow into a capillary-driven Washburn-type flow could be observed and reproduced by an analytical solution.

We used laboratory multi-inlet experiments similar to those in the former studies by Kordilla et al. (2017) to establish continuous droplet or stable rivulet flow on a vertical smooth fracture plane. The aforementioned study focused on the effect of free-surface flow on the partitioning dynamics at a single fracture intersection. Flow on the vertical surface, since it has no opposing fracture wall, is dominated by inertial forces (Wood et al., 2005). In natural settings, free-surface flow may occur along dissolution shafts and wide-aperture fractures with widths of up to several millimeters, which have been measured in field experiments (e.g., Dahan et al., 2000; Salve et al., 2004).

In this work, the number of horizontal fractures was successively increased to $n_f = 2$ and 3 and aperture widths d_f remained large (1 and 2.5 mm). An exchange with a porous matrix did not occur because synthetic and nonporous materials were used. This allowed us to isolate and investigate processes affecting the mass partitioning for droplet and rivulet flows while approximating bulk behavior. The validity of the analytical solution for Washburn-type fracture inflow was tested in experiments with single and multiple fracture intersections and for both aperture widths. To enable further upscaling, we derived a transfer function to reproduce and predict partitioning processes during rivulet flow for extended fracture cascades.

Materials and Methods

Experimental Setup and Procedure

The fracture network consists of two to four vertically stacked custom-made cubes made out of clear poly(methyl methacrylate) (PMMA) with dimensions of 20 by 20 by 20 cm (Fig. 2). They are separated by metal spacers with a thickness d_f of 1 or 2.5 mm. The flatness of six different cube walls was measured using a depth

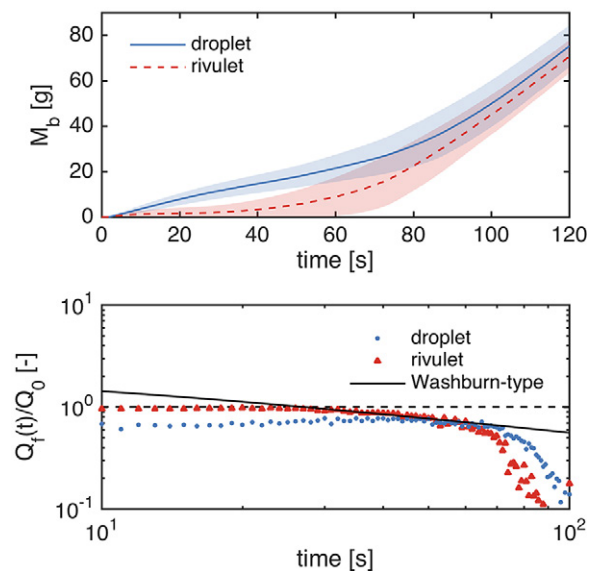


Fig. 1. Accumulated mass M_b that bypasses a horizontal fracture intersection (top) and normalized fracture inflow rates (bottom) vs. time in analog percolation experiments (after Kordilla et al., 2017). Two cubes are used with a vertical spacing d_f of 2.5 mm. Each line shows the ensemble mean of 20 experiments. Shaded areas display standard deviations. The black line represents the analytical solution for Washburn-type flow with the onset t_0 being 27 s.

goniometer on a 5- by 5-cm raster, where deviations from a perfectly planar surface showed a maximum amplitude of 1.27 mm for a single cube wall. The mean height difference between measured values on six randomly chosen cube walls and their midpoint acting as reference datum is 0.05 ± 0.19 mm. The static contact angle for sessile droplets with an average volume of 1.74 ± 0.12 μL was determined using a contact angle goniometer. The partially wetting substrate exhibited a contact angle θ_0 of $65.2 \pm 2.9^\circ$.

During the experiment, distilled water was drawn via silicone tubes with an inner diameter of 1.5 mm using a microprocessor-controlled 24-channel laboratory dispenser (Ismatec IPC High Precision Multichannel Dispenser ISM934C). Frequent calibration of the dispenser ensured constant flow rates throughout the experiments without pulsation of flow induced by the planetary drive. It should be noted that in some of the figures, dye has been used to enhance visual clarity; however, it was not added during the experiments to avoid alterations of the fluid's physical properties (Timmons et al., 1971). The water was directed to the top of one side of the uppermost cube across an equally spaced array of inlets. Two different stable flow regimes were established while keeping the total volumetric flow rate, Q_0 , constant at 15 mL min^{-1} : (i) stable low meandering rivulet flow prevailing via an injection of $3 \times 5 \text{ mL min}^{-1}$, or (ii) an input of $15 \times 1 \text{ mL min}^{-1}$ producing consecutive droplets. Findings from Dragila and Weisbrod (2003) showed a switch from capillary droplet mode to film flow in a vertical analog fracture due to an increase in atmospheric pressure. However, the injection rates applied in this study were chosen to clearly separate the two regimes.

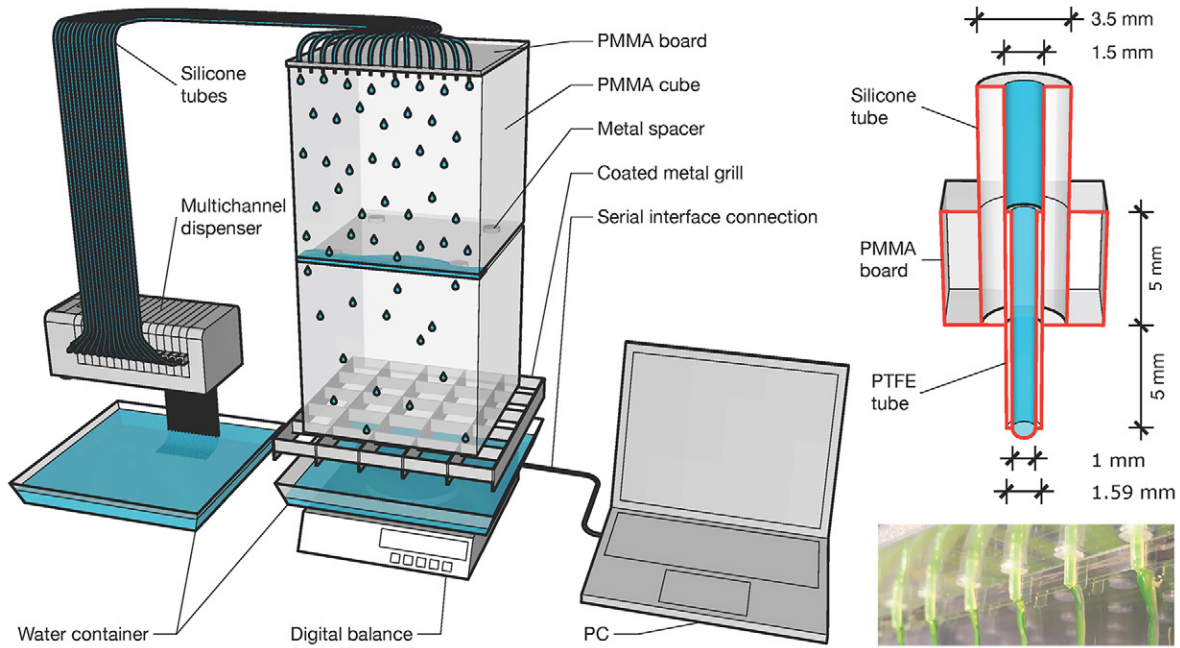


Fig. 2. Sketch of the laboratory setup used in our multi-inlet analog percolation experiments (left) and injection nozzle (right). Cubes are 20 by 20 by 20 cm. PMMA is poly(methyl methacrylate); PTFE is polytetrafluoroethylene.

The sequence of cubes was placed on a metallic square grill with a cell size of 5 by 5 by 5 cm that was coated with a hydrophobic lacquer ($\theta_0 \approx 110^\circ$) to allow fast transmission of the percolating water to the drip pan below. A digital laboratory balance (Kern EG 2200–2NM) measured real-time data of the accumulated weight, M_b , on the drip pan with an accuracy of 0.01 g. A delay of the arrival time of ≈ 400 ms, due to the distance between the bottom of the lowest cube and the drip pan, was captured using a camera at $240 \text{ frames s}^{-1}$. This produced no discernible impact on the collected results. Additionally, evaporation rates were experimentally determined to be $\approx 0.05 \text{ g min}^{-1}$ for a fully wetted surface of the drip pan at 20°C . However, despite these rates being far less than the total injection flow rates ($\approx 0.3\%$), travel time distributions were corrected for weight losses.

Note that the PMMA material does not offer a porous matrix for capillary-driven fluid uptake due to a negative matrix potential. Furthermore, all the fractures were well connected, resulting in no air pressure variation in vertical and horizontal fractures. Thus, the uniformly advancing fluid front led to no air pockets being trapped in the horizontal fracture. This is an idealized scenario for infiltration via unsaturated fracture networks in karst systems that, however, allows for the systematic investigation of mass partitioning at fracture intersections and the impact of the fracture cascade on the output (recharge) signal at the bottom.

Theoretical Methods

The total volumetric flow rate $Q_0 \text{ [L}^3 \text{ T}^{-1}\text{]}$ applied at the top of the setup was identical for each flow mode. Hence, the total mass M in the fracture network at time t is given by

$$M(t) = Q_0 t \quad [1]$$

The total mass is divided between the horizontal fractures (and on the vertical surfaces) and the drip pan at the bottom of the setup:

$$M(t) = M_f(t) + M_1(t) \quad [2]$$

where M_f is the mass stored in the fractures and M_1 is the accumulated mass on the drip pan. The volumetric fracture inflow rate $Q_f \text{ [L}^3 \text{ T}^{-1}\text{]}$ is obtained by derivation of Eq. [2], which gives

$$\frac{dM(t)}{dt} = Q_0 = \frac{dM_f(t)}{dt} + \frac{dM_1(t)}{dt} \quad [3]$$

Therefore, the volumetric fracture inflow rate is given by

$$Q_f(t) = \frac{dM_f(t)}{dt} = Q_0 - Q_1(t) \quad [4]$$

where we define $Q_1(t) = dM_1(t)/dt$. Figure 1 shows that for rivulet flow, initially all the flow occurs inside the fracture because $Q_f = Q_0$. This is different for the droplet mode, in which water is more likely to initially bypass the fracture. Flow in the horizontal fracture is dominated by capillary forces. In the rivulet mode, water is initially drawn in at the rate Q_0 at which it is provided. At a certain time t_0 , the flow in the fracture starts decreasing slowly until a characteristic saturation time, after which Q_f decreases exponentially fast. Note that the times are offset by the travel time from the fracture to the drip pan, which occurs when the flow starts partitioning at the fracture intersections. In this sense, the time t_0 marks the time of first fluid arrival at the drip pan. The slow initial decrease after time t_0 may be explained by Washburn-type capillary flow, as detailed by Kordilla et al. (2017). In the following, we briefly summarize the model and discuss it in the context of multiple fractures.

Washburn-Type Fracture Inflow

After an initial time period in which water is drawn into the fracture, limited only by the total flow rate, the fracture flow rate decreases because the pressure gradient that drives the flow, this means the (capillary) pressure drop across the penetration length, decreases. This decrease may be captured by the Washburn law (Bell and Cameron, 1905; Washburn, 1921) for a planar fracture. Along these lines, the penetration length $l(t)$ is obtained by combining Poiseuille's law for planar fractures with an expression for the differential fluid volume in the element of $dl(t)$:

$$\frac{dl(t)}{dt} = \frac{d_f^2 \Delta P_c}{4\eta l(t)} \quad [5]$$

where η is viscosity and ΔP_c is capillary pressure. Solving Eq. [5] for the initial length $l(t = t_0) = l_0$ gives

$$l(t) = l_0 \sqrt{1 + \frac{d_f^2 \Delta P_c}{2\eta l_0^2} (t - t_0)} \quad [6]$$

The fluid mass within the fracture is $M_f(t) = A_f l(t) \rho_w$, where ρ_w is the density of water and A_f is the area of the fracture cross-section. Note that this applies to an idealized uniform penetration front, which in general is not the case. Thus, the flow rate into the fracture according to Eq. [4] is

$$Q_f(t) = \frac{Q_0}{\sqrt{1 + 2k_f(t - t_0)}} \quad [7]$$

where we set $k_f = d_f^2 \Delta P_c / 2\eta l_0^2$. This behavior can be observed in Fig. 1 in a relatively narrow time interval between the onset of Washburn-type flow and a cut-off time, which is given by the time when the fracture is filling up. As we will see in the following, for the interpretation of fluid arrival at the bottom of the setup, the dominant characteristics are the onset and cutoff times due to the fact that the outlet signal can be seen as the convolution of the contributions from individual fractures.

Transfer Function Approach

We now consider the outflow rate at the bottom of the setup in the context of linear response theory or transfer function theory (Jury et al., 1986). Thus, the output signal $Q_{n+1}(t)$ at the bottom of the n th building cube of the setup is given in terms of the input signal $Q_n(t)$ at the top as

$$Q_{n_f}(t) = \int_0^t \varphi_{n_f}(t - t') Q_{n_f-1}(t') \quad [8]$$

where $\varphi_{n_f}(t)$ is the transfer function that accounts for vertical film flow and flow partitioning into the horizontal fracture in the n th cube. For the setup with a single fracture discussed above, this relation reads as

$$Q_1(t) = Q_0 \int_0^t dt' \varphi(t') \quad [9]$$

Thus, the transfer function is related to the flow rate at the drip pan and within the fracture as

$$\varphi(t) = \frac{dQ_1(t)}{dt} = -\frac{dQ_f(t)}{dt} \quad [10]$$

Consequently, the transfer function is characteristic of the flow in the horizontal fracture. In principle, as indicated in Eq. [8], the transfer function may depend on the (flow) properties of each cube, which is in fact the case for the first cube in the droplet flow mode, as discussed above. In the rivulet flow mode, we assume that the flow partitioning dynamics in each cube are the same and can be characterized by a single transfer function, which according to Eq. [10] can be estimated from the output signal at the bottom of the second cube or alternatively from an imbibition experiment in a single planar fracture. In this study, we used the first method as discussed below. Relation Eq. [10] and Fig. 1 imply that the transfer function is zero for times smaller than the onset of the Washburn-type flow, then grows to a maximum after which it decreases exponentially fast. To capture these main features, we use the truncated Gaussian

$$\varphi(t) \propto \frac{\exp\left[-(t - \mu)^2 / 2\sigma^2\right]}{\sqrt{2\pi\sigma^2}} \quad [11]$$

where μ denotes the time of the maximum and σ^2 the width of the Gaussian, which may be approximated by the difference between the onset time of the Washburn regime and the cutoff time. Note that the transfer function is normalized to 1, hence

$$\int_0^\infty dt \varphi(t) = 1 \quad [12]$$

The transfer function approach for the total fracture flow gives Q_{f,n_f} after n_f fractures:

$$Q_{f,n_f}(t) = Q_0 \left[1 - \int_0^t dt_{n_f-1} \varphi(t - t_{n_f-1}) \dots \int_0^{t_3} dt_2 \varphi(t_3 - t_2) \int_0^{t_2} dt_1 \varphi(t_2 - t_1) \varphi(t_1) \right] \quad [13]$$

Results and Discussion

Partitioning Dynamics at Unsaturated Fracture Intersections

Sliding droplets exhibit a range of dynamic behavior on the open fracture plane before moving into a fracture or accumulating on the drip pan. While this work mainly deals with rivulets, which occur at higher discharge rates, the fluid–substrate and hence the wetting properties can be characterized following Podgorski et al. (2001), who identified linear relationships between capillary number Ca and Bond number Bo . Ghezzehei (2004) adopted this scaling to characterize fluid–substrate systems using two parameters, γ and Δ_0 , which depend on fluid parameters (surface tension and viscosity) and wetting properties, i.e., adhesive thresholds:

$$Ca = \gamma Bo \cos(\alpha) - \Delta_0 \quad [14]$$

The surfaces used in this work and water as a fluid exhibit two distinct linear scaling regimes for two tested inclination angles α (45 and 90°) and a range of droplet sizes. Up to Bond numbers of ≈ 1.2 ($\gamma = 5.3 \times 10^{-4}$ and $\Delta_\theta = -5 \times 10^{-4}$), droplets show a spherical cap geometry. For higher Bond numbers, that is, larger droplets and/or higher inclination angles, elongated droplets occur, which may partially emit smaller droplets at their tails, and values of $\gamma = 4.68 \times 10^{-3}$ and $\Delta_\theta = -5.72 \times 10^{-3}$ were determined.

The partitioning of the arriving water mass at an unsaturated fracture intersection depends on the prevailing force balance of inertial, gravitational, viscous, and capillary forces acting on the fluid. Figure 3 shows a selection of common partitioning phenomena. While the fracture is completely unsaturated, a drop may bypass the gap between two cubes (Fig. 3a). If the drop is large and fast enough to develop an elongated tail (e.g., after coalescence of two sliding drops), it is likely to contribute a part of its mass to filling of the fracture (Fig. 3b). Once a sliding drop encounters and connects to the stored fluid, its own mass is either partially or completely taken up into the fracture (Fig. 3c). Less common observations include sliding drops that stop on the vertical plane on top of the fracture opening. A drop may also hydraulically connect to the liquid in the fracture without being drawn into the aperture. A consecutive drop will attach to the overhanging liquid mass. In both cases, most mass bypasses the fracture. The most efficient fracture inflow can be observed when the prevailing flow regime consists of stable rivulets (Fig. 3d). Once the inlet and horizontal fracture are hydraulically connected, a quickly advancing fluid front can be observed where essentially no mass bypasses the horizontal fracture. Once the horizontal fracture is fully saturated, it acts as a source for new rivulets on the following vertical PMMA plane. In contrast to the well-controlled inlet with three individual streams, the number of new rivulets may be lower (increase of flow rate per rivulet) and lead to meandering dynamics (Schmuki and Laso, 1990). However, flow rates are not high enough to cause the rivulets to dynamically oscillate, hence a stable connection between the inlet and the horizontal fracture is guaranteed. As additional horizontal fractures are encountered, this process is repeated once the liquid has fully saturated the next fracture.

Results from experiments are presented for both droplet and rivulet flows in terms of the accumulated mass M_b (Fig. 4) over time. The number of cubes was varied to create settings with either one, two, or three consecutive horizontal fractures. Therefore, the time for the experiments was successively extended to capture the switch to steady-state conditions. We considered two different fracture widths, 1 and 2.5 mm. Two stages in the temporal evolution can be distinguished:

1. For droplet flows and a single fracture intersection ($n_f = 1$), water accumulates at a higher rate on the digital scale than with rivulet flow; that is, the bypass efficiency is higher.
2. Once the fracture is fully saturated, M_b increases linearly as the total inflow rate equals the discharge onto the drip pan.

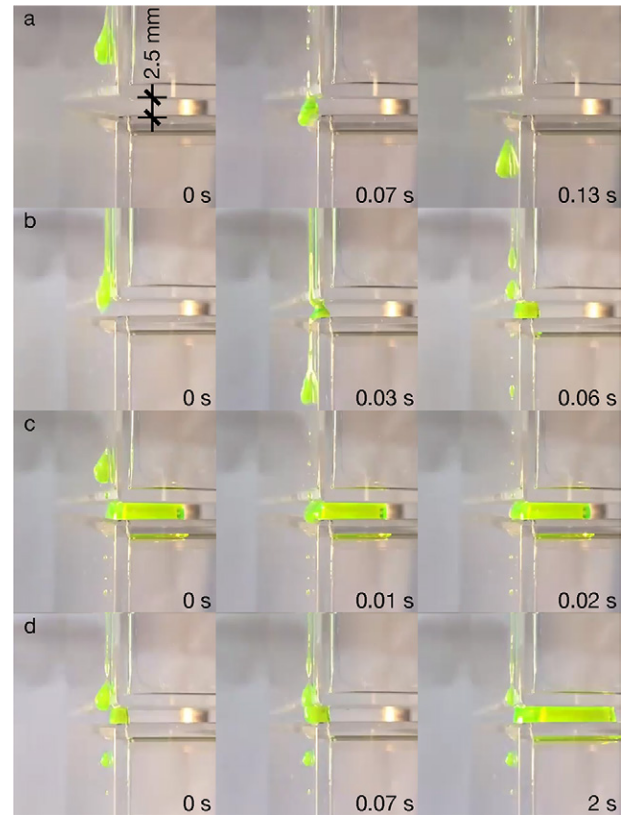


Fig. 3. Sliding droplets approaching an unsaturated fracture intersection may either (a) bypass it, (b) partially penetrate it, or (c) completely contribute to its filling; (d) a rivulet establishes a hydraulic connection between inlet and fracture while efficiently filling it.

The transition between these stages is completed later during droplet flow and is further delayed by increasing aperture widths d_f from 1 to 2.5 mm and growing fracture cascades as the total fracture volume increases. The difference in the bypass efficiency of both flow regimes persists, where $n_f > 1$. However, even if the inlet condition favors the formation of droplets, after every consecutive horizontal fracture the likelihood of droplets on the vertical plane diminishes, leading to a convergence with the characteristic repetitive fracture filling of experiments where rivulet flows are induced at the inlet.

Capillary-Driven Fracture Inflow

Figure 5 shows normalized fracture inflow rates Q_f/Q_0 for all experiments presented above. Following Eq. [7], the analytical solution for Washburn-type fracture inflow is fitted to the measured data, with parameters t_0 and k_f shown in Fig. 6. During droplet flow with a single fracture, the normalized inflow rate is considerably lower than for rivulet flow (contrast is stronger than observed by Kordilla et al., 2017). For this case, the spread of data is too high to infer a transition into a Washburn-type fracture inflow. A good fit, on the other hand, is achieved where rivulet flow prevails for the case $n_f = 1$. As observed by Kordilla et al. (2017), flow occurs at short times only in the fracture until a Washburn-type flow is established, after which flow in the fractures decreases more

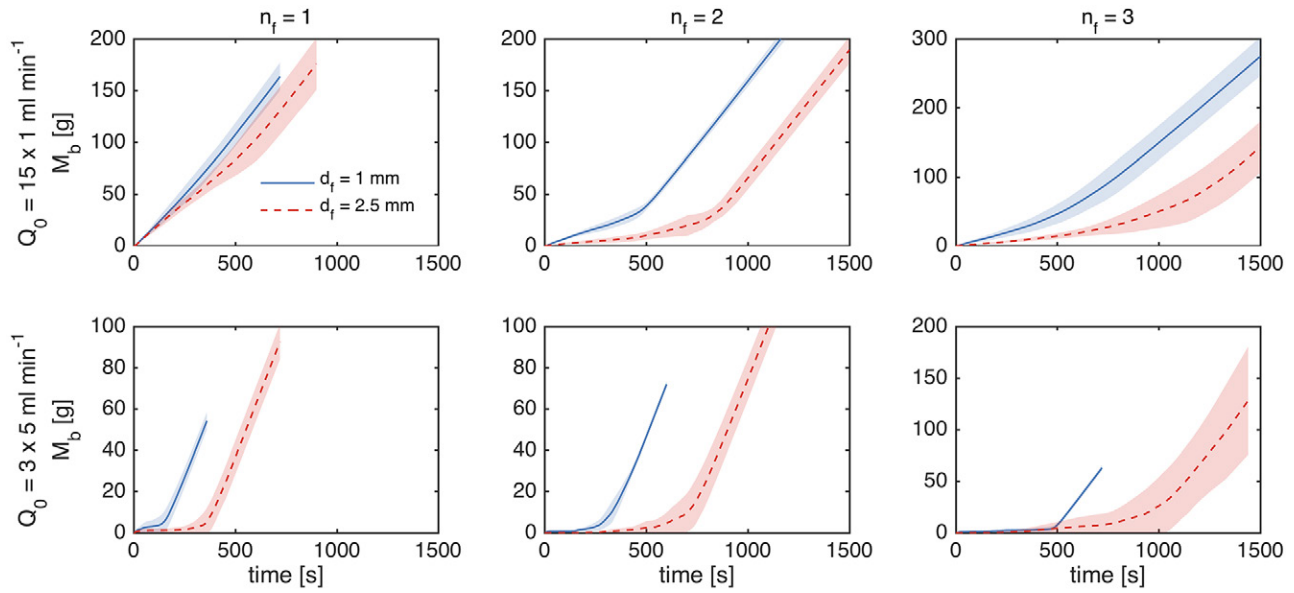


Fig. 4. Bypassing mass M_b vs. time for droplet (top) and rivulet flow (bottom) produced by a multi-inlet array. Fracture widths d_f are 1 and 2.5 mm. The number of fractures n_f is either one (left), two (middle), or three (right). Each line represents the ensemble mean values of 10 experiments. Shaded areas display the respective standard deviations.

slowly than exponential. At larger times, when the fractures are close to full saturation, fracture flow decreases exponentially fast. The Washburn-type flow period is relatively short and comprises only $<1 \times 10^2$ s. The fracture flow is faster for $d_f = 1$ mm than for $d_f = 2.5$ mm because capillary forces in the fracture are stronger. Thus, the onset of Washburn-type flow occurs earlier. Note that the onset time t_0 actually marks the time of first fluid arrival at the drip pan, which occurs as flow starts partitioning at the fracture intersection. Overall, the time at which the fracture flow starts declining

from Q_0 increases with growth of the overall fracture volume, i.e., for increasing fracture width d_f and number of fractures n_f . The time of first arrival at the drip pan, or equivalently, the time at which $Q_{f,nf}$ starts decreasing, increases linearly with the number of fractures n_f as shown in Fig. 6. As the time of first arrival increases, the relative importance of the Washburn-type flow period decreases and flow is dominated by the onset time and the time until the exponential cutoff. In the following, we quantify the observed $Q_{f,nf}$ using the transfer function approach described above.

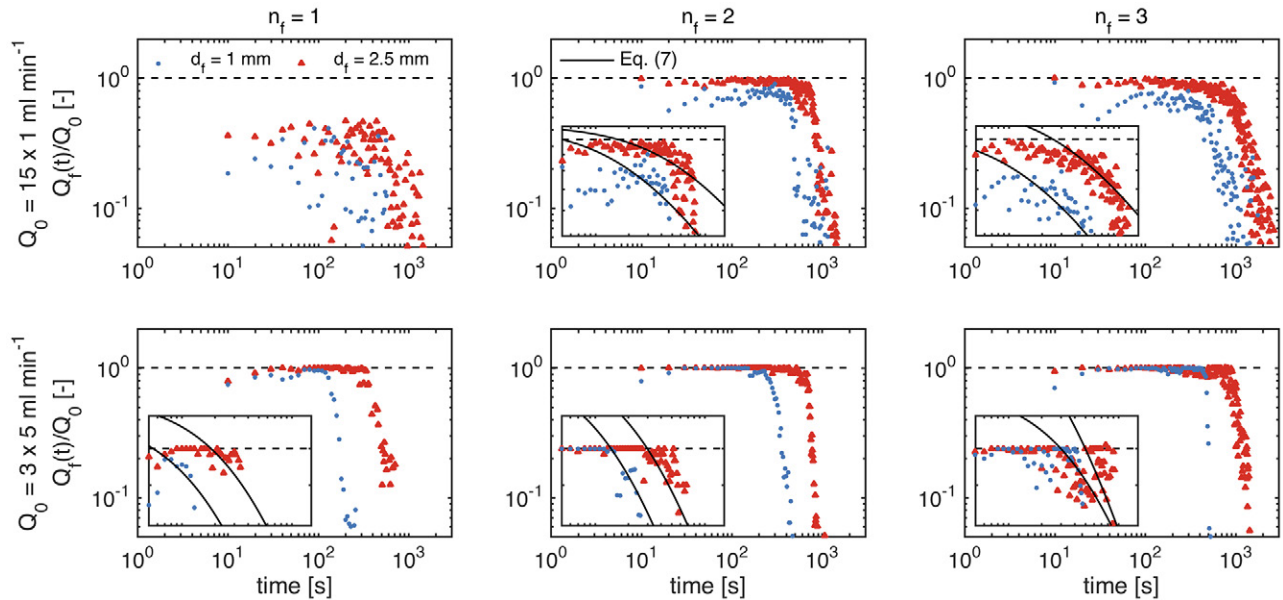


Fig. 5. Normalized fracture inflow rate Q_f/Q_0 for droplet (top) and rivulet flow (bottom) produced by a multi-inlet array. Results show average values of 10 experiments for each aperture width d_f and number of fractures n_f . Insets show fitted Eq. [7] between 5×10^1 and 1.5×10^2 s and have a y axis range from 5×10^{-1} to 1.1 (top) or from 8×10^{-1} to 1.1 (bottom).

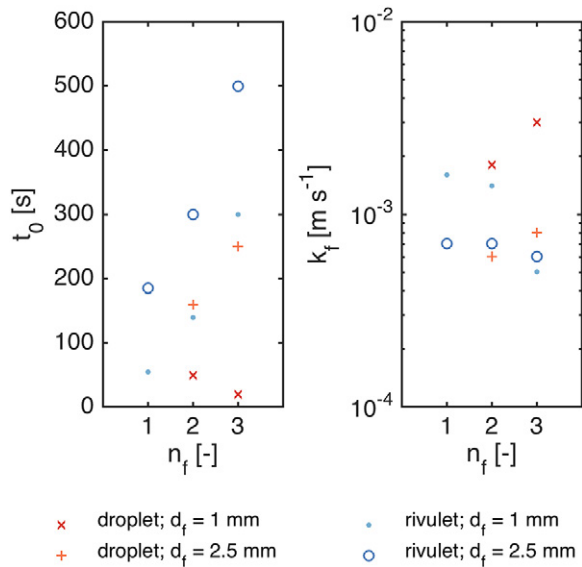


Fig. 6. Adjusted parameters of time of onset of Washburn-type flow t_0 and Washburn transition constant k_f to fit Eq. [7] to multi-inlet experiments.

Transfer Function

The transfer function φ is obtained by fitting the Gaussian Eq. [11] to the numerical derivative of the flow rate $Q_1(t)$ for a single fracture so that the resulting output signal approximates the measured data. Figure 7 shows φ for mass partitioning during rivulet flow at a fracture intersection with aperture widths of 1 and 2.5 mm.

During the initial stage of the experiments, we can briefly observe fluid bypassing the fracture before stable rivulets on the first horizontal plane are formed that connect inlet and fracture opening. This early overshoot is recognized by the balance and leads to a first peak of the transfer function. This effect is less apparent for larger aperture widths and growing fracture cascades. At full saturation [$Q_1(t) = Q_0$], the accelerated accumulation of water on the drip pan leads to a sudden increase of the output signal and marks the time when the most pronounced peak of the transfer function can be observed.

The continuous flow is interrupted when the rivulet reaches the bottom of the second cube and encounters the coated metal grill. Droplets form on the edges of the cube and grill until a critical mass is reached and the falling drops accumulate on the digital balance. Hence, the output signal is affected by these highly frequent pulses that overlap the continuous accumulation. However, the transfer function is obtained as a derivative of the flow rate (i.e., the derivative of the outflow mass with respect to time) with a coarser temporal discretization, i.e., it is not affected by the droplet accumulation and release. The low-frequency oscillatory behavior of the transfer function, specifically for a wider horizontal fracture (Fig. 7, bottom), is a result of the breakthrough process once the horizontal fracture is close to full saturation. Various flow regimes can shortly occur on the second vertical plane at this point, ranging

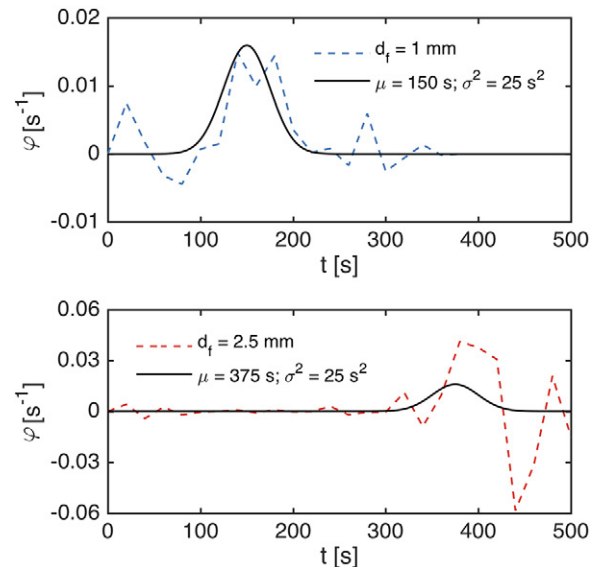


Fig. 7. Transfer functions φ obtained from measured data during rivulet flow at a single fracture intersection ($3 \times 5 \text{ mL min}^{-1}$, dashed lines) for fracture width d_f of 1 (top) and 2.5 mm (bottom) and the respective Gaussian distributions (solid lines) by which they are replaced.

from droplets to rivulets, which induce a pulsation of the outflow signal until an equilibrium in terms of the flow rate has been established again. This process is not explicitly taken into account by the Gaussian function.

In both cases, the variance σ^2 is 25 s^2 . The mean values μ are 150 s ($d_f = 1 \text{ mm}$) and 375 s ($d_f = 2.5 \text{ mm}$), which is in agreement with the factor by which the total fracture volume is increased. Figure 8, once more, shows the fracture inflow during rivulet flow alongside predictions obtained by Eq. [13]. The transfer function approach is in good agreement with the data and accurately reproduces the global flow behavior.

Conclusion

Our results confirm a considerably higher bypass efficiency of droplet flow on a vertical plane that is intersected by a single horizontal fracture compared with rivulet flow. This is much less apparent for a fracture cascade with $n_f > 1$ horizontal fracture intersections. In fact, for increasing n_f the travel time distributions obtained for inlets that enforce droplet flows converge to the travel time distributions obtained for inlets at which rivulet flows are induced. This observation can be explained as follows. At every additional horizontal fracture, a certain fraction of droplets enters the fracture. Horizontal fractures, however, are less likely to emit droplets (as opposed to the enforced inlet condition in the case of 15 inlets). These fractures can be seen as (dynamic) depth-dependent boundaries that emit preferentially rivulet flow. Thus, every consecutive horizontal fracture intersection increases the chance for the formation of rivulets. Therefore the proposed transfer function approach is likely to capture the infiltration correctly independent of the chosen initial boundary condition.

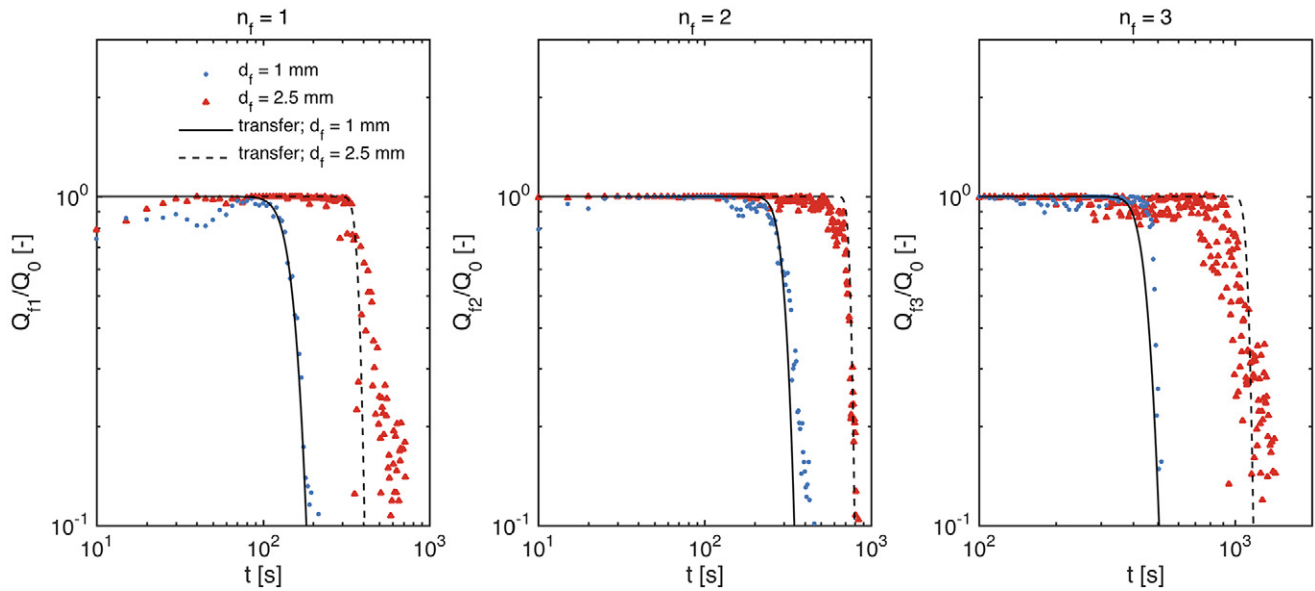


Fig. 8. Normalized fracture inflow rates Q_f/Q_0 for fracture widths d_f of 1 and 2.5 mm and number of fractures n_f of one (left), two (middle), or three (right) during rivulet flow with predictions calculated by Eq. [13].

The analytical solution for Washburn-type fracture inflow (Kordilla et al., 2017) is shown to reproduce our results obtained from experiments, where rivulet flow is the prevailing regime, but fails to describe the filling of a single fracture during droplet flow, where the onset of the capillary-driven flow type is delayed if the aperture width is increased.

The strictly sequential filling of unsaturated fractures during rivulet flow was successfully recovered by a Gaussian transfer function for up to three fracture intersections. Hence, it is shown to be a suitable tool to enable further upscaling of mass partitioning processes to arbitrary-sized fracture cascades.

While the PMMA material used in these experiments shows similar wetting properties to some geological materials, it cannot account for imbibition with a porous matrix. Furthermore, slight impurities and tiny defects of the substrate's surface, which some researchers relate to flow instabilities observed in experiments (e.g., Towell and Rothfeld, 1966), are difficult to avoid and affect contact angle hysteresis (de Gennes et al., 2004). Additionally, the chosen geometries were simplified to isolate single aspects of the partitioning process; however, such ideal orthogonal networks are unlikely to occur in natural settings.

Thus, it remains open to what extent these observations can be transferred to complex natural fracture systems and/or intermittent flows. While for steady flow we expect behavior similar to that observed in the experiments, for non-steady flows droplets may be emitted from horizontal fractures triggered by limited water supply due to snapping effects and fragmentation (Ghezzehei and Or, 2005). The flow regimes in the vertical and horizontal fractures depend on the fracture aperture. In our experiments, vertical flow is gravity driven while horizontal flow is capillary driven. In a natural fracture system with a distribution of fracture apertures, different flow modes may occur. For horizontal fractures with a

wide aperture, for example, film flow along the fracture ceiling may occur. The roughness of natural fractures may have an impact on imbibition into the horizontal fractures and thus on the transient storage behavior. We expect this to affect the shape of the transfer function but not the global convolution mechanism, which allows prediction of the arrival time distribution at the outlet based on the convolution of the input signal with the transfer functions' characteristic of subsequent fractures. The impact of fracture-matrix interactions on the flow behavior has been quantified in the literature by mobile-immobile domain models, which in principle can be incorporated in the transfer function approach used here.

Thus, while the presented experimental results provide some insight into flow partitioning at fracture intersections and the role of storage in the fracture cascade for the understanding of the arrival time distribution, further studies are required to investigate how geometric properties of natural fracture systems (roughness, fracture aperture, inclination) and material properties (wetting, contact angle dynamics, matrix-fracture interaction) impact on these processes and their predictability.

Variables

A_f	cross-sectional area of fracture aperture [L ²]
Bo	bond number
γ	proportionality constant
Ca	capillary number
c_f	parallel plate constant [L ² T ⁻¹]
Δ_θ	projection factor of surface tension
d_f	aperture width [L]
η	viscosity [M L ⁻¹ T ⁻¹]
θ_0	static contact angle
k_f	Washburn transition constant [L ² T ⁻¹]
l	length [L]
l_0	initial length [L]

μ	mean [T]
M	total water mass [M]
M_b	bypassing water mass [M]
M_f	water mass stored in fracture [M]
n_f	number of fractures
P_c	capillary pressure [$M L^{-1} T^{-2}$]
Q_0	volumetric flow rate [$L^3 T^{-1}$]
Q_f	fracture inflow rate [$L^3 T^{-1}$]
ρ	density [$M L^{-3}$]
σ	surface tension [$M T^{-2}$]
σ^2	variance [T^2]
t	time [T]
t_0	onset of Washburn-type flow [T]
φ	transfer function [T^{-1}]

Acknowledgments

This work was funded by the Deutsche Forschungsgemeinschaft (DFG; German Research Foundation) under Grant no. KO 53591/1-1 and supported by the Open Access Publication Funds of the University of Göttingen. Marco Dentz acknowledges the funding from the European Research Council under the European Union's Seventh Framework Programme (FP7/2007-2013)/ERC Grant Agreement no. 617511 (MHetScale).

References

- Bell, J.M., and F.K. Cameron. 1905. The flow of liquids through capillary spaces. *J. Phys. Chem.* 10:658–674. doi:10.1021/j150080a005
- Bodvarsson, G.S., T.M. Bandurraga, and Y.S. Wu. 1997. The site-scale unsaturated zone model of Yucca Mountain, Nevada, for the viability assessment. Yucca Mountain Characterization Project Rep. LBNL-40376, UC-814. Earth Sci. Div., Lawrence Berkeley Natl. Lab., Berkeley, CA.
- Dahan, O., R. Nativ, E.M. Adar, B. Berkowitz, and Z. Ronen. 1999. Field observation of flow in a fracture intersecting unsaturated chalk. *Water Resour. Res.* 35:3315–3326. doi:10.1029/1999WR900198
- Dahan, O., R. Nativ, E.M. Adar, B. Berkowitz, and N. Weisbrod. 2000. On fracture structure and preferential flow in unsaturated chalk. *Groundwater* 38:444–451. doi:10.1111/j.1745-6584.2000.tb00231.x
- de Gennes, P.-G., F. Brochard-Wyart, and D. Quere. 2004. *Capillarity and wetting phenomena*. Springer, New York. doi:10.1007/978-0-387-21656-0
- Dietrich, P., R. Helmig, M. Sauter, H. Hötzel, J. Königter, and G. Teutsch, editors. 2005. *Flow and transport in fractured porous media*. Springer, Berlin. doi:10.1007/b138453
- Dippenaar, M.A., and J.L. Van Rooy. 2016. On the cubic law and variably saturated flow through discrete open rough-walled discontinuities. *Int. J. Rock Mech. Min. Sci.* 89:200–211. doi:10.1016/j.ijrmms.2016.09.011
- Dragila, M.I., and N. Weisbrod. 2003. Parameters affecting maximum fluid transport in large aperture fractures. *Adv. Water Resour.* 26:1219–1228. doi:10.1016/j.advwatres.2003.09.002
- Evans, D.D., and T.C. Rasmussen. 1991. *Unsaturated flow and transport through fractured rock related to high-level waste repositories*. Tech. Rep. US Nucl. Regul. Comm., Washington, DC.
- Faybishenko, B., S.M. Benson, and J.E. Gale, editors. 2015. *Fluid dynamics in complex fractured-porous systems*. Geophys. Monogr. Ser. John Wiley & Sons, Hoboken, NJ.
- Ghezzehei, T.A. 2004. Constraints for flow regimes on smooth fracture surfaces. *Water Resour. Res.* 40:W11503. doi:10.1029/2004WR003164
- Ghezzehei, T.A., and D. Or. 2005. Liquid fragmentation and intermittent flow regimes in unsaturated fractured media. *Water Resour. Res.* 41:W12406. doi:10.1029/2004WR003834
- Gunn, J. 1981. Hydrological processes in karst depressions. *Z. Geomorphol.* 25:313–331.
- Ji, S.H., M.J. Nicholl, R.J. Glass, and K.K. Lee. 2006. Influence of simple fracture intersections with differing aperture on density-driven immiscible flow: Wetting versus nonwetting flows. *Water Resour. Res.* 42:W10416. doi:10.1029/2006WR004953
- Jones, B.R., L.B. Brouwers, and M.A. Dippenaar. 2018. Partially to fully saturated flow through smooth, clean, open fractures: Qualitative experimental studies. *Hydrogeol. J.* 26:945–961. doi:10.1007/s10040-017-1680-3
- Jury, W.A., G. Sposito, and R.E. White. 1986. A transfer function model of solute transport through soil: 1. Fundamental concepts. *Water Resour. Res.* 22:243–247. doi:10.1029/WR022i002p00243
- Kordilla, J., T. Noffz, M. Dentz, T. Geyer, and A. Tartakovsky. 2017. Effect of unsaturated flow modes on partitioning dynamics of gravity-driven flow in a simple fracture intersection: Laboratory study and three-dimensional smoothed particle hydrodynamics simulations. *Water Resour. Res.* 53:9496–9518. doi:10.1002/2016WR020236
- LaViolette, R.A., R.J. Glass, T.R. Wood, T.R. McJunkin, K.S. Noah, R.K. Podgorney, R.C. Starr, and D.L. Stoner. 2003. Convergent flow observed in a laboratory-scale unsaturated fracture system. *Geophys. Res. Lett.* 30:10–12. doi:10.1029/2002GL015775
- Li, J., C. Cherubini, T.S.A. Galindo, Z. Li, N. Pastore, and L. Li. 2018. Laboratory investigation of flow paths in 3D self-affine fractures with lattice Boltzmann simulations. *Energies* 11(1):168. doi:10.3390/en11010168
- Liu, H.H., R. Salve, J.S. Wang, G.S. Bodvarsson, and D. Hudson. 2004. Field investigation into unsaturated flow and transport in a fault: Model analyses. *J. Contam. Hydrol.* 74:39–59. doi:10.1016/j.jconhyd.2004.02.004
- Nicholl, M.J., and R.J. Glass. 2005. Infiltration into an analog fracture. *Vadose Zone J.* 4:1123–1151. doi:10.2136/vzj2004.0110
- Nimmo, J.R. 2012. Preferential flow occurs in unsaturated conditions. *Hydrol. Processes* 26:786–789. doi:10.1002/hyp.8380
- Podgorski, T., J.M. Flesselles, and L. Limat. 2001. Corners, cusps, and pearls in running drops. *Phys. Rev. Lett.* 87(3):036102. doi:10.1103/PhysRevLett.87.036102
- Salve, R., H.-H. Liu, P. Cook, A. Czarnowski, Q. Hu, and D. Hudson. 2004. Unsaturated flow and transport through a fault embedded in fractured welded tuff. *Water Resour. Res.* 40:W04210. doi:10.1029/2003WR002571
- Schmuki, P., and M. Laso. 1990. On the stability of rivulet flow. *J. Fluid Mech.* 215:125–143. doi:10.1017/S0022112090002580
- Timmons, D.R., C.K. Mutchler, and E.M. Sherstad. 1971. Use of fluorescein to measure the composition of waterdrop splash. *Water Resour. Res.* 7:1020–1023. doi:10.1029/WR007i004p01020
- Tokunaga, T.K., K.R. Olson, and J. Wan. 2005. Infiltration flux distributions in unsaturated rock deposits and their potential implications for fractured rock formations. *Geophys. Res. Lett.* 32:L05405. doi:10.1029/2004GL022203
- Towell, G.D., and L.B. Rothfeld. 1966. Hydrodynamics of rivulet flow. *AIChE J.* 12:972–980. doi:10.1002/aic.690120524
- Trinchero, P., R. Beckie, X. Sanchez-Vila, and C. Nichol. 2011. Assessing preferential flow through an unsaturated waste rock pile using spectral analysis. *Water Resour. Res.* 47:W07532. doi:10.1029/2010WR010163
- Tsang, C.-F., I. Neretnieks, and Y. Tsang. 2015. Hydrologic issues associated with nuclear waste repositories. *Water Resour. Res.* 51:6923–6972. doi:10.1002/2015WR017641
- Washburn, E.W. 1921. The dynamics of capillary flow. *Phys. Rev.* 17:273–283. doi:10.1103/PhysRev.17.273
- Williams, P.W. 2008. The role of the epikarst in karst and cave hydrogeology: A review. *Int. J. Speleol.* 37:1–10. doi:10.5038/1827-806X.37.1.1
- Wood, T.R., and H. Huang. 2015. Experimental and modeling studies of episodic air–water two-phase flow in fractures and fracture networks. In: B. Faybishenko et al., editors, *Fluid dynamics in complex fractured porous systems*. John Wiley & Sons, Chichester, UK. p. 209–228.
- Wood, T.R., M.J. Nicholl, and R.J. Glass. 2002. Fracture intersections as integrators for unsaturated flow. *Geophys. Res. Lett.* 29(24):2191. doi:10.1029/2002GL015551
- Wood, T.R., M.J. Nicholl, and R.J. Glass. 2005. Influence of fracture intersections under unsaturated, low-flow conditions. *Water Resour. Res.* 41:W04017. doi:10.1029/2004WR003281